The Greenland Sea Jet: A mechanism for wind-driven sea ice export through Fram Strait

J. H. van Angelen,[1] M. R. van den Broeke,[1] and R. Kwok[2]

Received 18 April 2011; revised 11 May 2011; accepted 11 May 2011; published 28 June 2011.

[1] We present a mechanism for wind-driven sea ice export from the Arctic Ocean through Fram Strait for the period 1979–2007, using the output of a high-resolution regional atmospheric climate model. By explicitly calculating the components of the atmospheric momentum budget, we show that not large scale synoptic forcing (LSC), but mainly thermal wind forcing (THW) causes the persistent northerly jet (the Greenland Sea Jet) over Fram Strait. The jet results from horizontal temperature gradients in the atmospheric boundary layer (ABL), set up between cold ABL-air over the sea ice covered western Greenland Sea and the relatively warmer ABL over the ice-free eastern Greenland Sea. From 1993 onwards we find a negative trend in THW, due to a stronger response to climate warming of the ABL over the sea ice covered ocean, compared to that over the ice free ocean. Although on average LSC is smaller than THW, year to year variations in LSC explain most of the interannual variability in the sea ice area flux through Fram Strait (R = 0.81). A small positive trend is found for LSC, partly compensating the decrease in THW in recent years. **Citation:** van Angelen, J. H., M. R. van den Broeke, and R. Kwok (2011), The Greenland Sea Jet: A mechanism for wind-driven sea ice export through Fram Strait, *Geophys. Res. Lett.*, *38*, L12805, doi:10.1029/2011GL047837.

1. Introduction

[2] Sea ice forms an important component of the Arctic climate system. It reflects a significant amount of incoming solar radiation, limits the interaction between ocean and atmosphere and the relatively fresh meltwater impacts ocean circulation. Since the start of continuous observations in 1979 [*Johannessen et al.*, 2004; *Parkinson and Cavalieri*, 2008], Arctic sea ice extent has strongly decreased, especially in summer with record low values in 2005 and 2007 [*Comiso*, 2006; *Comiso et al.*, 2008]. Recent years also saw a decline in winter ice extent [*Comiso*, 2006], with a record low January 2011 extent of 13.55×10^6 km^2, 8.5% less than the 1979–2000 average (http://nsidc.org).

[3] Although direct melt also is a significant factor [*Kwok and Cunningham*, 2010], export through Fram Strait (FS) is the dominant sink for Arctic sea ice [*Kwok et al.*, 2004; *Kwok*, 2009]. Variations in sea ice export are related to the surface pressure gradient over FS [*Hilmer et al.*, 1998; *Harder et al.*, 1998; *Kwok et al.*, 2004; *Koenigk et al.*, 2006; *Tsukernik et al.*, 2009; *Vinje*, 2001], motivating several studies that investigated the relation between FS sea ice export and variability in atmospheric circulation patterns. No consistent relations were found between the North Atlantic Oscillation (NAO) [*Jung and Hilmer*, 2001; *Kwok et al.*, 2004], the Arctic Oscillation (AO) [*Rigor et al.*, 2002; *Wu et al.*, 2006], cyclone activity [*Brümmer et al.*, 2001, 2003] and FS sea ice export. None of these studies completely explained the persistent west-east pressure gradient over Fram Strait, with the associated northerly geostrophic wind over the Greenland Sea (GS) (Figure 1a).

[4] Here, we explicitly resolve the components of the lower atmospheric momentum budget over the GS region, to provide a theoretical framework for year to year variations in wind-driven sea ice export through FS. For this, we use output of the high resolution regional atmospheric climate model RACMO2.1/GR [*van Meijgaard et al.*, 2008], for the period 1979–2007, and yearly averaged sea ice area flux data through FS (1979–2007) [*Kwok*, 2009]. The next section briefly describes the climate model output and sea ice data used. The calculation of the momentum budget components is also discussed. Section 3 gives results of the momentum budget components and the relation to sea ice export. Conclusions are given in section 4.

2. Methods

2.1. Data

[5] For this study we use output of the regional atmospheric climate model RACMO2.1/GR for the period 1979–2007 [*van Meijgaard et al.*, 2008]. Figure 1a shows the full model domain, covering Greenland and its surrounding oceans. RACMO2.1/GR is a hydrostatic model, has a horizontal grid spacing of 11 km and 40 sigma levels in the vertical. The quality of the model output has been extensively evaluated by *Ettema et al.* [2010], and the model has been successfully used for atmospheric boundary layer studies in Antarctica [*van den Broeke et al.*, 2002; *van den Broeke and van Lipzig*, 2003; *van de Berg et al.*, 2008] and Greenland [*van Angelen et al.*, 2011]. RACMO2.1/GR is forced at the lateral boundaries by ECMWF reanalysis (ERA-40) data every 6 hours [*Uppala and Kållberg*, 2005]. From August 2002 onwards, operational data of the ECMWF are used. Sea ice cover and sea surface temperature are also prescribed from ERA-40.

[6] Yearly averaged (September to October) sea ice area fluxes through FS for the 1979–2007 period were determined by combining sea ice motion and sea ice concentration retrievals from satellite data [*Kwok*, 2009]. The average area flux of sea ice through FS is 706×10^3 km^2, with a standard deviation of 113×10^3 km^2. The uncertainty in the annual estimates is 28×10^3 km^2.

[1]Institute for Marine and Atmospheric Research Utrecht, Utrecht University, Utrecht, Netherlands.
[2]Jet Propulsion Laboratory, California Institute of Technology, Pasadena, California, USA.

0094-8276/11/2011GL047837

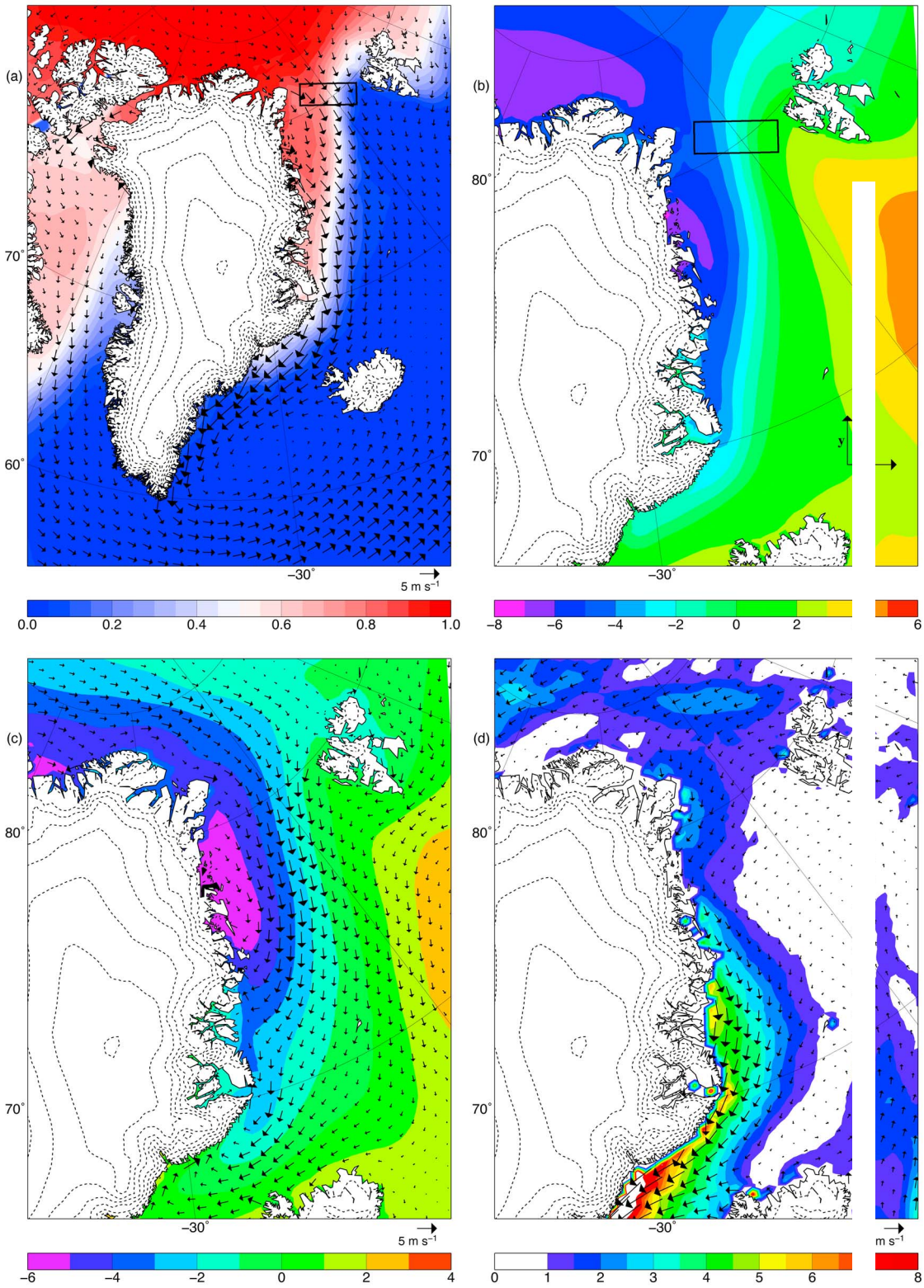

Figure 1. Average (1979–2007) (a) sea ice concentration (color) and near-surface winds. (b) Surface temperature perturbation [K]; (c) vertically integrated temperature perturbation [10^3 Km] and geostrophic winds associated with THW forcing and (d) LSC forcing [ms^{-1} h^{-1}] and associated geostrophic winds. The squares in Figures 1a and 1b define the FS area as used in this study. Dashed contours are 400 m surface elevation intervals. Wind vectors are plotted every 20th model grid point.

2.2. Momentum Budget

[7] Over a flat surface, the momentum budget in the x-direction can be approximated as follows:

$$\frac{\partial U}{\partial t} = \overbrace{-U\frac{\partial U}{\partial x} - V\frac{\partial U}{\partial y}}^{\text{HADV}} - \underbrace{W\frac{\partial U}{\partial z}}_{\text{VADV}} + \underbrace{\frac{g}{\theta_0}\frac{\partial \hat{\theta}}{\partial x}}_{\text{THW}} + \underbrace{fV}_{\text{COR}} - \underbrace{fV_{LSC}}_{\text{LSC}} - \underbrace{\frac{\partial \overline{uw}}{\partial z}}_{\text{FDIV}}, \quad (1)$$

with U and V the wind velocity components in the x- and y-direction, and θ_0 the background potential temperature, which is calculated by linearly extrapolating the potential temperature in the free troposphere towards the surface. $\hat{\theta}$ is defined as the vertically integrated temperature perturbation of the temperature deficit layer (TDL):

$$\hat{\theta}(z) = \int_z^{h_f} \Delta_\theta(z)dz, \quad (2)$$

with $\Delta_\theta(z) = \theta(z) - \theta_0(z)$, the temperature perturbation. h_f is chosen well above the TDL top in the free atmosphere. For this study we adopted the coordinate system as used in the RACMO2.1/GR model; U wind is in the x-direction as displayed in Figure 1a and not the easterly component. In this paper we present results for the lowest model layer at approximately 7 m above the surface.

[8] Equation (1) contains two active forcing components, the thermal wind (THW) and the large scale (LSC) forcing. Near the surface, LSC depends on the strength and direction of the flow above the TDL (U_{LSC} and V_{LSC}) and on the vertical gradient in the background potential temperature (θ_0) via the thermal wind balance. THW is driven by horizontal gradients in $\hat{\theta}$, i.e., horizontal gradients in the 'cold content' of the TDL. *van Angelen et al.* [2011] provides a detailed discussion of LSC, THW, θ_0 and $\hat{\theta}$ over the larger Greenland region. The other terms (horizontal and vertical advection (HADV, VADV), the coriolis force (COR) and momentum flux divergence (FDIV)) are passive forces, i.e., they only become important once flow has been initiated.

3. Results

3.1. Vertical Profiles

[9] Figure S1 of the auxiliary material shows average vertical profiles of θ and θ_0 (Figure S1a), U and V (Figure S1b) and the momentum budget components (Figure S1c) over FS for the period October 1999 to September 2000.[1] θ starts to deviate from θ_0 approximately 2.5 km above the surface (Figure S1a), signifying the large depth of the TDL. This is also the level where U and V start to deviate from their large scale components (Figure S1b). Large scale winds in the free troposphere are from the southwest and become near-zero close to the surface. In the free troposphere, the momentum budget (Figure S1c) shows a simple geostrophic balance. Closer to the surface, however, the momentum budget is dominated by THW, which drives a persistent northerly jet over FS and the Greenland Sea. Figure 1a clearly identifies this boundary-layer jet (70–85°N), which from now on we will refer to as the Greenland Sea Jet (GSJ).

3.2. Momentum Budget

[10] Figure 1b shows the average surface temperature perturbation (Δ_θ) over the region of interest. The strongest negative perturbations are found over the sea ice, with values of up to −7 K along the North and Northeast coast of Greenland; cold air from the ice sheet transported by katabatic winds [*van Angelen et al.*, 2011] accumulates over the sea ice covered ocean, and can maintain its low temperature owing to the insulating properties of the sea ice. Δ_θ increases away from the coast, reaching positive values of up to 5 K over the eastern Greenland Sea, where the ocean surface is sea ice free throughout the year. Here, the air is colder than the relatively warm sea surface, leading to a positive temperature perturbation at the surface.

[11] The vertically integrated temperature perturbation $\hat{\theta}$ (Figure 1c) shows the same features, with a pool of cold air over the Western Greenland Sea. The associated gradient in $\hat{\theta}$ results in THW forcing of up to 2 ms^{-1} h^{-1}. If balanced by COR, this forces a northerly geostrophic near-surface wind of up to 5 ms^{-1}, representing the GSJ. The GSJ is strongest over FS and the central Greenland Sea, coinciding with the boundary between the sea ice covered and sea ice free ocean (Figure 1a).

[12] Figure 1d displays LSC and the associated geostrophic wind. Although LSC is important in the higher atmosphere (Figure S1b), it is on average small near the surface in the FS region, less than 2 ms^{-1} h^{-1}. LSC becomes large along the east coast further south, which explains the far southward extent of sea ice along the east coast of Greenland, and is in agreement with the findings during the Greenland Flow Distortion Experiment [*Petersen et al.*, 2009].

[13] Figure 2a shows that yearly averaged total forcing in the x-direction (THW + LSC) is a very robust predictor of the yearly averaged wind in the y-direction (V) over FS. V varies between 1 and 5 ms^{-1}, and this interannual variability is fully explained by variations in total forcing (R = 0.98). The seasonal variability in V is pronounced (Figure 2b), with strongest southward winds in winter up to 5 ms^{-1} and a weak northward flow in summer (1 ms^{-1}). This seasonality can be ascribed to both THW and LSC forcing, with a dominant contribution of THW (Figure 2b). In summer, a combination of less sea ice cover along the Greenland coast and weaker katabatic winds from the ice sheet, diminishes the accumulation of cold air in this region [*van Angelen et al.*, 2011]. As a result the gradient of $\hat{\theta}$ in the offshore direction is small, resulting in a weaker or absent GSJ.

3.3. Sea Ice Area Flux Through FS

[14] Figure 2c shows the correlation and Figure 3a the correlation field of yearly averaged V with the sea ice area flux through FS. Correlation magnitude is largest over the eastern FS, close to Svalbard. Correlations are strong over the entire Greenland Sea, indicating a single forcing, in this case the GSJ. Figures 3b and 3c display correlation fields of yearly sea ice fluxes, LSC and THW. THW is the dominant forcing of the GSJ; it is also rather constant from year to year, in contrast to LSC. As a result, no significant correlation exists of THW with the sea ice flux (Figure 3b). Figure 3c shows that year to year variations in sea ice flux can be mainly ascribed to variations in LSC, with correlation in the FS > 0.8 (Figure 2d). By definition, LSC near the surface and in the upper air are strongly connected. As a

[1] Auxiliary materials are available in the HTML. doi:10.1029/2011GL047837.

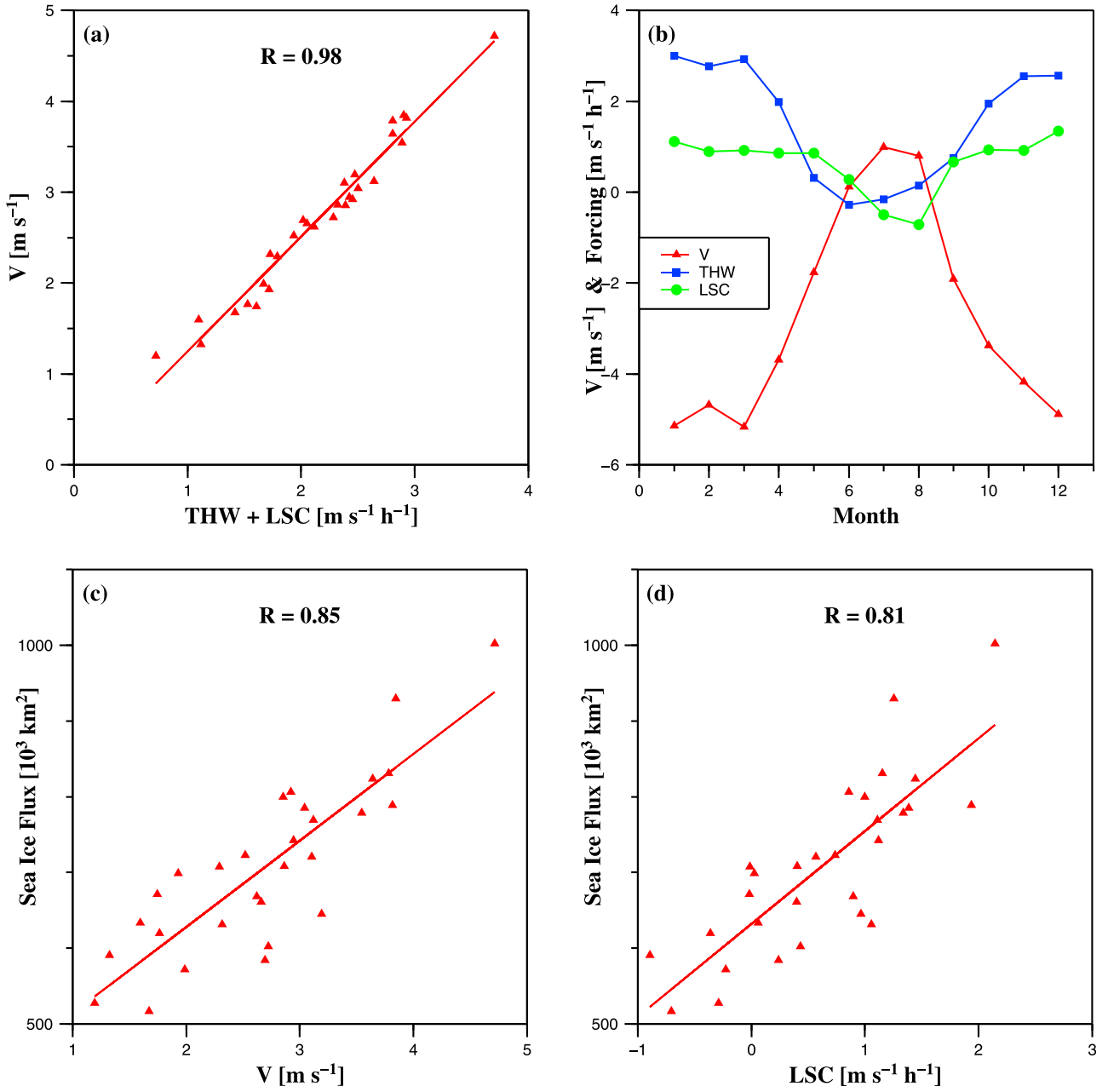

Figure 2. (a) Yearly average values over FS for wind forcing vs. wind speed, (b) average seasonal variation in V, THW and LSC, (c) yearly average values for windspeed vs. sea ice flux and (d) yearly average values for LSC vs. sea ice flux.

result, correlations between LSC at ~5000 m elevation and sea ice flux through FS is still strong (Figure 3d). Compared to the surface, the center of action has shifted to the west a result of the average westward tilt of the pressure field with height in response to the large scale SE-NW temperature gradient over Greenland. These results are not sensitive to the size or location of the FS averaging window.

3.4. Temporal Variability

[15] Figure 4 shows 1979–2007 time series of annual total sea ice fluxes through FS and annual average THW and LSC: No significant trend in sea ice export is present; interannual variability is large (σ = 16%) and driven by LSC (red line);THW (blue line) is relatively constant from year to year. The pool of cold air that sets up THW is continuously replenished by katabatic winds flowing off the ice sheet, which is a rather steady phenomenon in NE Greenland [*van Angelen et al.*, 2011]. Moreover, large scale winds that may disperse the cold air are weak in this region (Figure 1d).

[16] Between 1979 and 1993, THW is rather constant and significantly larger than LSC. From 1993 onwards, a downward trend in THW is visible, which is significant at the 99% significance level. This trend is the result of the different response of the ABL to upper air warming over a sea ice covered ocean, compared to a sea ice free ocean. Figure 4b compares the temperature trend over the west and east side of FS, close to the surface and at 500 hPa (for the definition of the east and west side of FS, see Figure S2). Upper air temperatures show a strong increase of +0.9 K/decade from 1993 onwards, both on the west and on the east side of FS. Close to

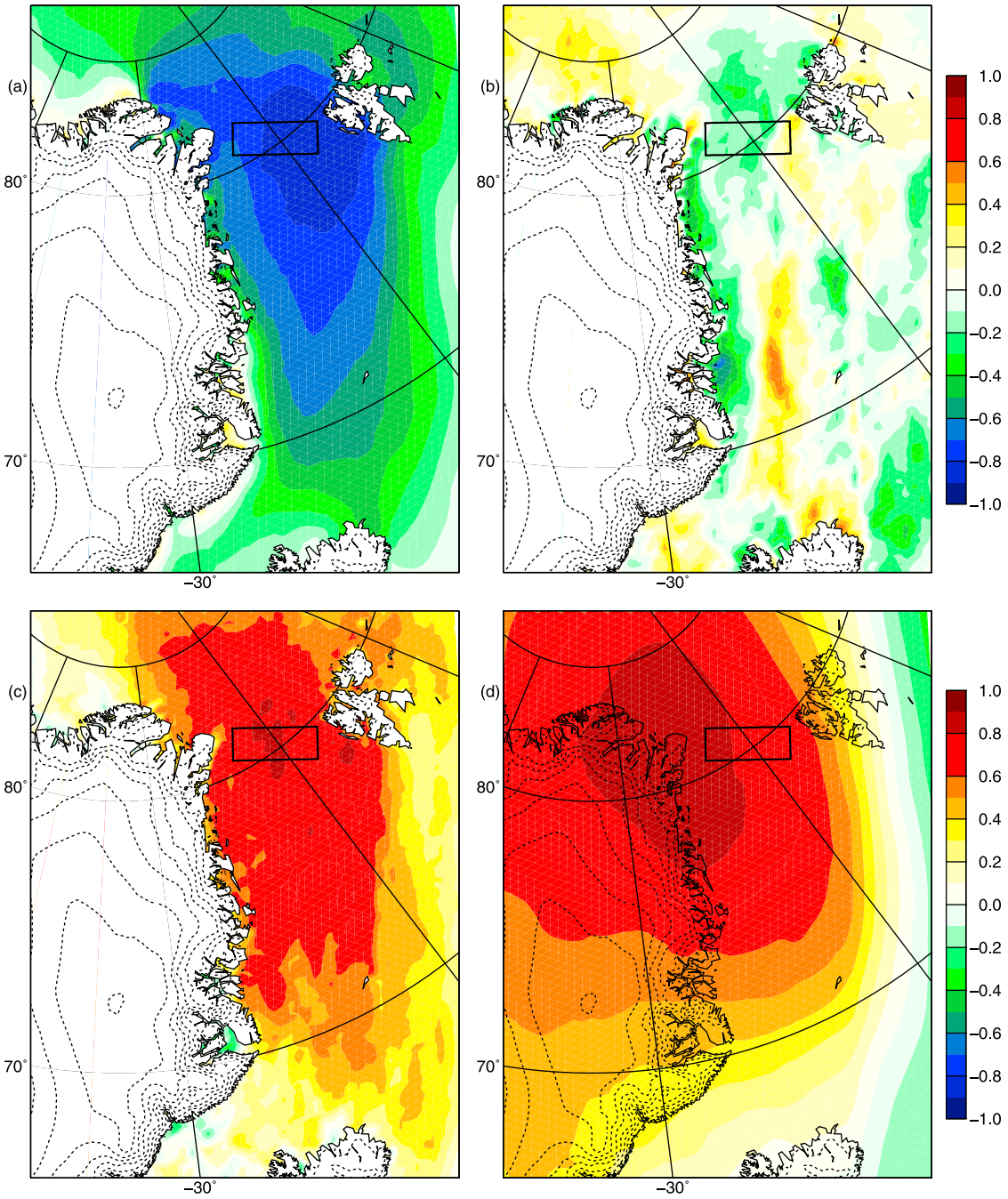

Figure 3. Correlation fields of annual total sea ice flux through FS with: (a) V (wind in the y-direction), (b) thermal wind forcing (THW) near the surface, (c) large scale forcing (LSC) near the surface, and (d) large scale forcing in the free troposphere (~5000 m height).

the surface, temperature trends are much more variable. Over the almost continuously sea ice covered west side of FS we find a positive trend of +0.7 K/decade (similar to the upper air trend), compared to a negative trend of −0.4 K/decade on the east side. This negative trend is the result of a small increase in sea ice cover in recent years over the east side of FS, limiting the heating of the ABL by the ocean. As a result of this differential heating over FS, the gradient in $\hat{\theta}$ is reduced, leading to a weakening of THW. Temperature trends for the entire region are shown in Figure S2. In general, temperature trends are strongest over sea ice covered regions (up to +1.5 K/decade), whereas over the ice free ocean trends are reduced due to the large heat capacity of the ocean water column. These findings are in agreement with the strong surface heating in the Arctic region in wintertime and reduced heating in summertime [*Graversen et al.*, 2008], as a result of the seasonality in sea ice cover. The weakening of THW is partly compensated by a (less significant) positive trend in LSC.

4. Conclusions

[17] These results show that FS sea ice export is maintained by the GSJ, forced by the pooling of cold air, that

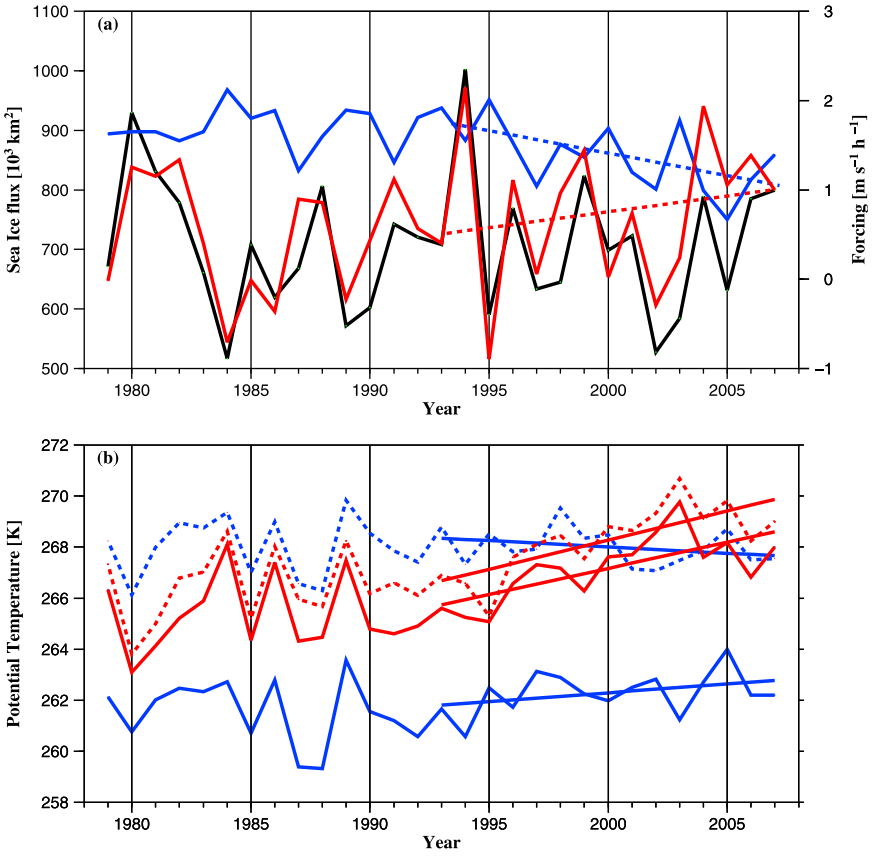

Figure 4. Yearly averaged values for (a) sea ice flux through Fram Strait (black), LSC (red) and THW(blue) and (b) yearly averaged temperature at 500 hPa (red) and near the surface (blue) over the western (solid) and eastern (dashed) FS.

originates from the Greenland ice sheet, over sea ice in the western GS, and the absence of this pooling further east over the open ocean. This implicates that in the absence of sea ice in FS, or when the FS was uniformly covered by sea ice, the southward transport by the GSJ would be less efficient, which is qualitatively supported by the absence of THW in summer. This represents a negative feedback of Arctic sea ice decline.

[18] The fact that the atmospheric boundary layer plays a pivotal role in FS sea ice transport implicates that thermal adjustment with the surface is important in explaining long term variability. In the case of the rapidly warming free atmosphere over the GS and Greenland, this has led to a weakening of the THW over FS, which represents another negative feedback on Arctic Sea ice loss.

[19] **Acknowledgments.** The Editor thanks the two anonymous reviewers for their assistance in evaluating this paper.

References

Brümmer, B., G. Müller, B. Affeld, R. Gerdes, M. Karcher, and F. Kauker (2001), Cyclones over Fram Strait: Impact on sea ice and variability, *Polar Res.*, *20*(2), 147–152, doi:10.1111/j.1751-8369.2001.tb00050.x.

Brümmer, B., G. Müller, and H. Hoeber (2003), A Fram Strait cyclone: Properties and impact on ice drift as measured by aircraft and buoys, *J. Geophys. Res.*, *108*(D7), 4217, doi:10.1029/2002JD002638.

Comiso, J. C. (2006), Abrupt decline in the Arctic winter sea ice cover, *Geophys. Res. Lett.*, *33*, L18504, doi:10.1029/2006GL027341.

Comiso, J. C., C. L. Parkinson, R. Gersten, and L. Stock (2008), Accelerated decline in the Arctic sea ice cover, *Geophys. Res. Lett.*, *35*, L01703, doi:10.1029/2007GL031972.

Ettema, J., M. van den Broeke, E. van Meijgaard, and W. van de Berg (2010), Climate of the Greenland ice sheet using a high-resolution climate model, part 1: Evaluation, *Cryosphere*, *4*, 511–527, doi:10.5194/tc-4-511-2010.

Graversen, R., T. Mauritsen, M. Tjernström, and E. Källén (2008), Vertical structure of recent Arctic warming, *Nature*, *541*(3), 53–56, doi:10.1038/nature06502.

Harder, M., P. Lemke, and M. Hilmer (1998), Simulation of sea ice transport through Fram Strait: Natural variability and sensitivity to forcing, *J. Geophys. Res.*, *103*(C3), 5595–5606, doi:10.1029/97JC02472.

Hilmer, M., M. Harder, and P. Lemke (1998), Sea ice transport: A highly variable link between Arctic and North Atlantic, *Geophys. Res. Lett.*, *25*(17), 3359–3362, doi:10.1029/98GL52360.

Johannessen, O., et al. (2004), Arctic climate change: Observed and modelled temperature and sea ice variability, *Tellus, Ser. A*, *56*, 328–341, doi:10.1111/j.1600-0870.2004.00060.x.

Jung, T., and M. Hilmer (2001), The link between the North Atlantic Oscillation and Arctic sea ice export through Fram Strait, *J. Clim.*, *14*, 3932–3943, doi:10.1175/1520-0442(2001)014<3932:TLBTNA>2.0.CO;2.

Koenigk, T., U. Mikolajewicz, H. Haak, and J. Jungclaus (2006), Variability of Fram Strait sea ice export: Causes, impacts and feedbacks in a coupled climate model, *Clim. Dyn.*, *26*, 17–34, doi:10.1007/s00382-005-0060-1.

Kwok, R. (2009), Outflow of Arctic Ocean sea ice into the Greenland and Barents seas: 1979–2007, *J. Clim.*, *22*, 2438–2456, doi:10.1175/2008JCLI2819.1.

Kwok, R., and G. F. Cunningham (2010), Contribution of melt in the Beaufort Sea to the decline in Arctic multiyear sea ice coverage: 1993–2009, *Geophys. Res. Lett.*, *37*, L20501, doi:10.1029/2010GL044678.

Kwok, R., G. F. Cunningham, and S. S. Pang (2004), Fram Strait sea ice outflow, *J. Geophys. Res.*, *109*, C01009, doi:10.1029/2003JC001785.

Parkinson, C. L., and D. J. Cavalieri (2008), Arctic sea ice variability and trends, 1979–2006, *J. Geophys. Res.*, *113*, C07003, doi:10.1029/2007JC004558.

Petersen, G., I. Renfrew, and G. Moore (2009), An overview of barrier winds off southeastern Greenland during the Greenland Flow Distortion Experiment, *Q. J. R. Meteorol. Soc.*, *135*(645), 1950–1967, doi:10.1002/qj.455.

Rigor, I., J. Wallace, and R. Colony (2002), Response of sea ice to the Arctic Oscillation, *J. Clim.*, *15*, 2648–2663, doi:10.1175/1520-0442(2002)015<2648:ROSITT>2.0.CO;2.

Tsukernik, M., C. Deser, M. Alexander, and R. Tomas (2009), Atmospheric forcing of Fram Strait sea ice export: A closer look, *Clim. Dyn.*, *35*(7), 1349–1360, doi:10.1007/s00382-009-0647-z.

Uppala, S., and P. Kållberg (2005), The ERA-40 re-analysis, *Q. J. R. Meteorol. Soc.*, *131*(612), 2961–3012, doi:10.1256/qj.04.176.

van Angelen, J. H., M. R. van den Broeke, and W. J. van de Berg (2011), Momentum budget of the atmospheric boundary layer over the Greenland ice sheet and its surrounding seas, *J. Geophys. Res.*, *116*, D10101, doi:10.1029/2010JD015485.

van de Berg, W., M. van den Broeke, and E. van Meijgaard (2008), Spatial structures in the heat budget of the Antarctic atmospheric boundary layer, *Cryosphere*, *2*, 1–12, doi:10.5194/tc-2-1-2008.

van den Broeke, M., and N. van Lipzig (2003), Factors controlling the near-surface wind field in Antarctica, *Mon. Weather Rev.*, *131*, 733–743, doi:10.1175/1520-0493(2003)131<0733:FCTNSW>2.0.CO;2.

van den Broeke, M., N. van Lipzig, and E. van Meijgaard (2002), Momentum budget of the East Antarctic atmospheric boundary layer: Results of a regional climate model, *J. Atmos. Sci.*, *59*, 3117–3129, doi:10.1175/1520-0469(2002)059<3117:MBOTEA>2.0.CO;2.

van Meijgaard, E., L. van Ulft, W. van de Berg, F. Bosveld, B. van den Hurk, G. Lenderink, and A. Siebesma (2008), The KNMI regional atmospheric climate model RACMO version 2.1, *Tech. Rep. 302*, R. Neth. Meteorol. Inst., De Bilt.

Vinje, T. (2001), Fram Strait ice fluxes and atmospheric circulation: 1950–2000, *J. Clim.*, *14*, 3508–3517, doi:10.1175/1520-0442(2001)014<3508:FSIFAA>2.0.CO;2.

Wu, B., J. Wang, and J. Walsh (2006), Dipole anomaly in the winter Arctic atmosphere and its association with sea ice motion, *J. Clim.*, *19*, 210–225, doi:10.1175/JCLI3619.1.

R. Kwok, Jet Propulsion Laboratory, California Institute of Technology, Mail Stop 300-331, 4800 Oak Grove Dr., Pasadena, CA 91109, USA.

J. H. van Angelen and M. R. van den Broeke, Institute for Marine and Atmospheric Research Utrecht, Utrecht University, Princetonplein 5, NL-3584 CC Utrecht, Netherlands. (j.h.vanangelen@uu.nl)